Geotechnical behaviour of low-permeability soils in surfactant enhanced electrokinetic remediation

RUBEN LÓPEZ-VIZCAÍNO[1*], VICENTE NAVARRO[2], JUAN ALONSO[2], ANGEL YUSTRES[2], PABLO CAÑIZARES[1], MANUEL A. RODRIGO[1] and CRISTINA SÁEZ[1]

[1]*Department of Chemical Engineering, Facultad de Ciencias y Tecnologías Químicas, University of Castilla-La Mancha, Ciudad Real, Spain*

[2]*Geoenvironmental Group, Civil Engineering School, University of Castilla-La Mancha, Ciudad Real, Spain*

---

*Address correspondence to Dr. Rubén. López-Vizcaíno, Department of Chemical Engineering, Facultad de Ciencias y Tecnologías Químicas, University of Castilla-La Mancha, Campus Universitario s/n,13071 Ciudad Real, Spain; Tel.: +34902204100 Ext. 6309; Fax: 926295256

E-mail: ruben.lopezvizcaino@uclm.es / r.lopezvizcaino@gmail.com

Abstract

Electrokinetic processes provide the basis of a range of very interesting techniques for the remediation of polluted soils. These techniques consist on the application of a current field in the soil that develops different transport mechanisms capable of mobilizing several types of pollutants. However, the use of these techniques could generate non desirable effects related to the geomechanical behavior of the soil, reducing the effectiveness of the processes. In the case of the remediation of polluted soils with plasticity index higher than 35, an excessive shrinkage can be observed in remediation test. For this reason, the continued evaporation that takes place in sample top can lead to the development of cracks, distorting the electrokinetic transport regime, and consequently, the development of the operation. On the other hand, when analyzing silty soils, in the surroundings of injection surfactant wells, high seepages can be generated that give rise to the development of piping processes. In this article methods are described to allow a reduction, or to even eliminate, both problems.

Keywords: Low-permeability soils; electrokinetic remediation; cracked soil; piping process

Introduction

The development of industrial and agricultural activities has supposed a source of many different pollutants that have been leaked into soils and groundwater. Many of these contaminants produce a serious environmental problem, and even could be hazardous for humans or animals if ingested through polluted water extracted from wells or springs.

Some in-situ remediation techniques have been tried throughout the last decades to eliminate the pollutants from both soils and groundwater. Among them, the use of aqueous solutions has been successfully used in numerous processes of in situ flushing of contaminated soils. The efficiency of the remediation based on flushing depends on the hydraulic conductivity, being soils with high hydraulic conductivities (up to $1 \cdot 10^{-3}$ m/s), those that provide better results [1,2]. In the other hand, low-permeability soils, as argillaceous materials, presents a reduction of the effectiveness of these processes, due to the low flushing flow generated. For this reason, the use of these in-situ flushing techniques is little attractive. However, the use of electrokinetic remediation can be interesting [3]. This technology consists on the application of a low electrical current through inert electrodes, which are inserted in the soil or electrolyte wells [4]. The electrical field generated in the soil develops different electrokinetic transport processes such as electroosmosis, electromigration and electrophoresis, which are the responsible for the mobilize and remove the pollution from soil [5].

Although many studies have been performed related to electrokinetic remediation for different polluted soils [6-8], little work has been done related to the hydro-mechanical response of different soil types considered a priori suitable for these techniques due to their low hydraulic permeability. This paper focuses on some relevant aspects of their hydro-mechanical response during electrokinetic remediation, specifically in the description and the analysis of the problems related to cracking, and piping. For this purpose, tests were performed under realistic conditions, similar to those expected during field operations. The tests carried out consist of the decontamination of two different soils polluted with phenanthrene (Hydrophobic Organic Compound, HOC), used as a model of diesel spill, applying electrokinetic remediation enhanced with injection of surfactant.

Materials and methods

Materials

Two low-permeability soils have been used in this research work: a commercial micronized kaolin, and a soil coming from a quarry in Toledo (Spain) (Sagra soil). Table 1, shows the mineralogical analysis of the soils employed, which have been provided by the commercial suppliers. The mineral composition has been obtained by x-ray diffraction and thermal analysis (Differential Thermal Analysis, DTA; and Thermo-Gravimetry, TG).

These soils were homogeneously contaminated with phenanthrene (PHE), up to pollution level of 500 mg PHE kg^{-1} dry soil. As enhanced fluid remediation, sodium dodecyl sulphate solution, SDS (10 kg m^{-3}) was selected. The addition of SDS is necessary to increase the HOCs aqueous-phase concentration via micelle/microemulsion formation, or mobilization of the HOC phase [10-14].

Experimental Setup

All the electrokinetic tests were conducted in an electrokinetic remediation mock-up consisting of an electrokinetic reactor, power supply and tanks of electrolyte and surfactant. The description of this setup is described in literature in previous works [3, 4]. Experimental setup and a mock-up general scheme, with the location of the instrumentation are shown in Figure 1A and Figure 1B, respectively. The potential gradient (E_z) applied in all the tests was 1 V cm^{-1}. The behavior of soils were continuously monitored during the realization of the tests by quantification of liquid flows, temperatures, and soil moisture.

To ensure test conditions similar to those expected in the field, the soils considered were compacted to realistic "in situ" conditions, as the initial moisture (w_o) and dry density (ρ_d) shown in Table 2. These values were obtained from standard Proctor compaction tests [15]. The moisture (w) was analyzed by the Standard ASTM D2216 [16]. Grain density (ρ_s) was analyzed by the Standard ASTM D854 [17]. ρ_d, porous index (e), and porosity (n), degree of saturation (S_r) can be calculated by Equation 1-4, respectively.

$$\rho_d = \frac{mass\ of\ dry\ soil}{total\ volume} \quad (1)$$

$$e = \frac{\rho_s - \rho_d}{\rho_d} \quad (2)$$

$$n = \frac{e}{1+e} \quad (3)$$

$$S_r = \frac{\rho_d \cdot \rho_s \cdot w}{(\rho_s - \rho_d) \cdot \rho_w} \quad (4)$$

To ensure that the desired densities were reached a careful disposal/construction process was followed. Known amounts of mass of soil were prepared with the ratio of water and soil particles necessary to reach the optimal moisture content. Each known amount of soil was compacted in layers of 5 cm thickness until reaching a determined volume in the mock-up (Figure 2A). The volume that each known amount of soil had to occupy was previously known through an external graduation on the electrokinetic reactor. By this way, compacting with a normalized hammer mounted on a steel plate to provide a uniform transmission of the energy to the totality of the layer, a flat soil surface was practically reached. By reaching the proposed volume through compaction, the desired density was obtained in the soil samples. Once the operation of compaction was finished with one layer, a new layer is disposed. In order to verify the effectiveness in the preparation of the soil a series of samples were taken from the wells logged for anodic, cathodic and surfactant wells (Figure 2B) a very good agreement with the desired density was obtained.

The soils tested were classified from a textural point of view according to ASTM D2487. Sagra soil presents a high Plasticity index (PI=40) and it is classified as a high plasticity clay (CH), and Kaolin is a low plasticity silt (ML), according to the Unified Soil Classification System (USCS) chart [18].

Results and discussion

Desiccation Cracks

The appearance of cracks in clays during desiccation is a well-known phenomenon [18]. Its impact on the efficiency of clay barriers has been described by diverse authors, in special, in landfill liners [20-22]. The presence of desiccation cracks defines preferential flow paths, and faster movement of gas, water, solutes and particles than would be expected from the soil matrix properties [23]. As result of this fact, the hydraulic conductivity of cracked soils is usually orders of magnitude higher than that of intact soils[24,25]. The containment function of the clay can be jeopardized. Nevertheless, in electrokinetic remediation processes, the effect can be the opposite. The electroosmotic transport takes place in the proximity of solid particles [26-28]. Therefore, the appearance of cracks could suppose a loss of connectivity between the solid skeleton, reducing the electroosmotic flow. Consequently, it is of interest that cracks do not appear.

Desiccation cracks would occur if soil shrinkage is constrained, generating a tensile stress which exceeds the bonding strength of the soil particles [29]. As soil is a highly complex material, this process is controlled by a large number of factors. Although in the last years diverse models have been considered to describe and to quantify the phenomenon [30], the description of cracking and crack propagation is still not completely understood. However, from to qualitative point of view, the schematic description shown in Figure 3 provides a good approximation of the crack initiation process. As water evaporation proceeds, the soil water content is reduced. It is accompanied by an increase in matric suction and intergranular stress. Each particle on the layer surface suffers a tensile force. If this rising microscopic tensile stress exceeds the bonding strength, a crack occurs on the surface [23]. Therefore, the soil evaporation behaviour plays a main role in the soil cracking process. In electrokinetic tests the three conditions pointed out to ensure the persistence of evaporation from soils occur, namely: (i) a constant supply of heat to meet the latent head requirement (provided by the electrodes), (ii) the laboratory conditions usually ensures that the vapour pressure of the air in the laboratory atmosphere is lower than that of the soil surface, and (iii) a continuing supply of water (from the anode) to the evaporation surface (the top part of the soil sample, as well as the cracks themselves if they remain in unsaturated conditions).

In agreement with Daniel [22], a high shrinkage can be expected for soils with a plasticity index (PI) greater than 35, which could be taken as a reference value. In the tested mock-ups, this estimation was accomplished. No cracks appeared in “kaolin soil”, PI=13. Cracks appeared in “Sagra soil”, PI=40 (see Table 2). As it can be appreciated in Figure 4, cracks were located mainly between the anodic wells and the wells were surfactant was applied. During the first days of the test, this region was affected by an increment of the temperatures (see Figure 5). This fact favor water loss by evaporation. For this reason the initiation of cracks was focused on this region. Once cracks appeared, as indicated by Casagrande [26], the infiltration/gravitational and electroosmotic flows presents strong variation related with this phenomenon. Figure 6 shows the evolution of these flows.

It is noted that during the first 13 days, the gravitational flow (GF) is non-existent and the electroosmotic flow (EF) achieves the highest value (4.2×10^{-4} m^3 day^{-1}). After this moment, GF increases up to reach 3.9×10^{-3} m^3 day^{-1}, one order of magnitude higher than the maximum EF. In the other hand, the EF presents a continuous descend during the test up to stabilize in 2.4×10^{-5} m^3 day^{-1}. In comparison with results obtained in other studies [3-4], the EF obtained is very low, which means a reduction of efficiency of the electrokinetic treatment. These behaviors are related with the formation of cracks that favors an increment of the GF towards the granular layer in the bottom of the mock-up and reduces the water transported to the cathodic region by electroosmosis process. In order to minimize this problem, the following procedure was applied (Figure 7). First, the initial moisture of the superficial layer of soil was reestablished (Figure 7A). Second, the superficial cracks were filled up with a slurry prepared with the same soil of the mock-up (Figure 7B). Finally, a reduction of the evaporation rate was attempted. For this purpose a granular cover was arranged, as can be observed in Figure 7C, in order to work as capillary barrier to evaporation. The granular material placed was a coarse sand with an air entry pressure lower than 1 kPa. By this way, the sand remains unsaturated. Therefore, its hydraulic conductivity is significantly reduced, and the evaporation is highly complicated [4]. The use of this type of covers on landfill liners was analyzed with detail by Yanful et al. [31]. These authors analyzed evaporation in a clayey till sample (115 mm diameter, 125 mm height) after placing a coarse sand on the top (47 mm height). They verified that after placing the coarse sand the cumulative evaporation after twelve days of test was reduced from 31.2 mm to 18.9 mm (40% reduction). The volumetric water content did not decrease in the clayey soil, which practically remained saturated. For this reason, the matric suction was barely modified, and the risk of development of desiccation cracks disappeared.

When dismantling the mock-up, the sand cover was removed, and it was verified that cracks that had been refilled before remained closed. There were not new cracks either, therefore, the disposal of a granular cover was effective. Nevertheless, although after the soil improvement described in the previous paragraph gravity flow was reduced considerably, this continued being high throughout the test (see Figure 6). Probably, internal cracks were generated, and it was not possible to seal them completely.

In order to check this assumption, some verifications were carried out. First, it must be considered that the average value of gravimetric flow, 8.5×10^{-4} m^3 day^{-1} (Figure 6), is associated to an average hydraulic conductivity of 3×10^{-8} m s^{-1}. This value is two orders of magnitude higher than the initial hydraulic conductivity of 2.29×10^{-10} m s^{-1} (see Table 2) obtained for the same soil in an oedometer test. In addition, as shown in Figure 8, the distribution of dry densities indicates very low values in the surroundings of the anode. This fact could be related with a partial dissolution of some constituents of the soil matrix (calcite, for example), due to the transport of an acidic front around the anodic zone. This acidic front is produced by the combination of two electrochemical processes: the generation of protons in the reaction of water anodic oxidation, and the movement of these protons through the soil by the electromigration process. The values showed in Figure 8 define an average ρ_d of 820 kg m^{-3} from an initial value of 1210 Kg m^{-3}. This suggest that the porosity of the soil was incremented by cracks. Moreover, it should be stressed that *Sr* of the Sagra soil was greatly reduced (Table 3). A reduction in *Sr* may indicate two events: a decrease of *w*, or an increment of *n*. In this case the *w* increased from 28.7 to 33.8%, thus reducing *Sr* must be related to an increase of *n* within the soil that is consistent with the increase in the *e* observed and the decrement of the ρ_d previously commented. Also, the fact that *Sr* has dropped by 22% is consistent with the high vertical flows obtained (Figure 6). All these aspects justify the existence of a macroporosity (cracks) inside the sample by the formation of internal cracks.

Therefore, in order to avoid this situation, a granular layer should be arranged to cover the soil surface before beginning the test. Otherwise, cracks will develop in plastic soils, and the representativeness of the tests could be conditioned.

Piping Processes

When water flows through a soil, the viscous forces associated to the flow produces a microscopic shear stress in the surface of the solid particles. If shear stress exceeds a certain threshold, the solid particles are eroded [32]. Conduits or preferential flow paths can be produced, working like “pipes”. For that reason, this phenomenon is known in a generic way as “piping”. The greater the velocity of flow, the greater the shear forces exerted. For that reason, microscopic shear is proportional to macroscopic seepage gradient. In the test configuration outlined in Figure 1A reduced water head gradients were induced. Therefore, erosion problems were not expected. However, after the tests the start of piping process was observed, as shown in Figure 9.

Piping only take place in the Kaolin mock-up (silt soil). This is consistent with the smaller resistance to the erosion and lower critical seepage gradient of this soil with respect to clay (see Table 4 [33]). Piping was located close to a well of surfactant. It must be considered that SDS, an ionic surfactant, caused an important gradient of osmotic pressure in the surroundings of surfactant wells. An osmotically driven water flow was activated from outside (soil) to inside (well), which according to Mitchell[28], it can be estimated by means of the Equation 5:

$$i_h = \omega \frac{R \cdot T}{\gamma_W} \frac{\Delta c}{\Delta r} \qquad (5)$$

where ω is the osmotic efficiency, R is the universal gas constant, T is the absolute temperature, γ_w is the unit weight of water, and Δc is the difference between the concentration inside the well and that in the soil pores at distance Δr from the well boundary. The osmotic efficiency is a measure of the degree to which the soil behaves as a perfect semipermeable membrane. If soil does so, ω is equal to one. However, if the 'membrane' is 'leaky', and water flows carrying with it some dissolved salts, ω is reduced, tending to zero [34]. In agreement with the values considered by Mitchell [29], for a moisture of 39.5% (final average value of the moisture in kaolin), and a Liquid Limit of 41.0 (Table 2), osmotic efficiency will be probably inferior to 10^{-4}. Even with this small value, the ratio Δc /Δr was very elevated since the variation of Δc took place after adding the surfactant at a reduced distance Δr. This gave rise to a value of i_h that, according to the estimative values in Table 4, resulted in the piping processes reflected in Figure 9.

In order to avoid piping process is advisable to dispose a granular material acting as a filter. For a given soil, a material fulfills the condition of filter if placed 'downstream' with respect the flow direction prevents the drag of its particles. As it is known, to meet this condition the granulometry of the filter-material must satisfy a series of requirements with regard to the granulometry of the soil to be protected. According to the indications given by the United States Bureau of Reclamation [35], since 100% of kaolinite particles are finer than 0.074 mm (see Figure 10), is due to use a filter that fulfills (Equation 6):

$$D_{15F} < Maximum(9 \cdot D_{85B}, 0.2\ mm) \qquad (6)$$

where D_{85B} defines a size of particle so that the 85% of particles of the kaolinite are inferior, whereas D_{15F} defines a size of particle so that only the 15% of particles of the filter are smaller. Since D_{85B} is approximately equal to 20 μm (see Figure 10), D_{15F} equal to 0.2 mm should be adopted.

To verify the validity of this value a surfactant well was reproduced. Using the same kaolin soil, two samples were prepared using the molds of a Normal Proctor test (see Figure 11A and 11B). The same surfactant, as used in the tests previously described, (SDS 10 kg m^{-3}) was added to the wells. But, whereas in the one of them the surfactant was added without placing a filter, a crown of 0.3 cm of external radio was prepared in the second with fine sand in which it was fulfilled that D_{15F}=0.2 mm. In the first case, the piping processes were again observed (Figure 11A). In the second case, the filter protected the soil, and it was not eroded by the osmotically driven water flow (Figure 11B).

Conclusions

Two geotechnical problems were identified during electrokinetic tests performed with different kinds of low-permeability soils polluted with phenanthrene. These problems were mainly related to the thermo-hydro-mechanical behavior of each particular type of soil, and the undesirable secondary effects that take place during electrokinetic of contaminated soils. Avoiding these problems is necessary for the efficiency of the process. The disposition of a sand layer, acting as a barrier to evaporation on the top of high plasticity soils susceptible to the development of cracks, and of a sand filter around the surfactant addition well in the case of soils susceptible to develop piping processes, reduces or even eliminates these problems.

Acknowledgements

This work has been supported by Spanish Government through the projects CTM2010-18833/TECNO and CTM2013-45612-R and INNOCAMPUS Program of the University of Castilla La Mancha. The experimental collaboration of Oscar Merlo is truly recognized.

References

[1] Mulligan, C.N.; Yong, R.N.; Gibbs, B.F. Remediation technologies for metal-contaminated soils and groundwater: an evaluation. Eng. Geol. **2001**, *60*, 193-207.

[2] Mulligan, C.N.; Yong, R.N.; Gibbs, B.F. Surfactant-enhanced remediation of contaminated soil: a review. Eng. Geol. **2001**, *60*, 371-380.

[3] Lopez-Vizcaino, R.; Saez, C.; Canizares, P.; Navarro, V.; Rodrigo; M.A. Influence of the Type of Surfactant on the Mobility of Flushing Fluids for Electro-Remediation Processes. Separ. Sci. Technol. **2011**, *46*, 2148-2156.

[4] López-Vizcaíno, R.; Sáez, C.; Mena, E.; Villaseñor, J.; Cañizares, P.; Rodrigo, M.A. Electro-osmotic fluxes in multi-well electro-remediation processes. J. Environ. Sci. Heal. A. **2011**, *46*, 1549-1557.

[5] Mena, E.; Rubio, P.; Canizares, P.; Villasenor, J.; Rodrigo, M.A. Electrokinetic transport of diesel-degrading microorganisms through soils of different textures using electric fields. J. Environ. Sci. Heal. A. **2012**, *47*, 274-279.

[6] Page, M.M.; Page, C.L. Electroremediation of contaminated soils. J. Environ. Eng-Asce. **2002**, *128*, 208-219.

[7] Saichek, R.E; Reddy, K.R. Electrokinetically enhanced remediation of hydrophobic organic compounds in soils: A review. Crit. Rev. Env. Sci. Tec. **2005**, *35*, 115-192.

[8] Alshawabkeh, A.N. Electrokinetic Soil Remediation: Challenges and Opportunities. Separ. Sci. Technol. **2009**, *44*, 2171-2187.

[9] Kile, D.E.; Chiou, C.T. Water solubility enhancements of ddt and trichlorobenzene by some surfactants below and above the critical micelle concentration. Environ. Sci. Technol. **1989**, *23*, 832-838.

[10] Edwards, D.A.; Luthy, R.G.; Liu, Z.B. Solubilization of polycyclic aromatic-hydrocarbons in micellar nonionic surfactant solutions. Environ. Sci. Technol. **1991**, *25*, 127-133.

[11] Ko, S.O.; Schlautman, M.A.; Carraway, E.R. Partitioning of hydrophobic organic compounds to sorbed surfactants. 1. Experimental studies. Environ. Sci. Technol. **1998**, *32*, 2769-2775.

[12] Wilson, D.J.; Clarke, A.N. Soil clean up by in situ surfactant flushing, IV. A two-component mathematical model. Sep. Sci. Technol, **1991**, *29*, 1177-1194.

[13] López-Vizcaíno, R.; Alonso, J.; Cañizares, P.; León, M.J.; Navarro, V.; Rodrigo, M.A.; Sáez, C. Electroremediation of a natural soil polluted with phenanthrene in a pilot plant. J. Hazard. Mater. **2014**, *265*, 142-150.

[14] López-Vizcaíno, R.; Alonso, J.; Cañizares, P.; León, M.J.; Navarro, V.; Rodrigo, M.A.; Sáez, C. Removal of phenanthrene from synthetic kaolin soils by eletrokinetic soil flushing. Sep. Purif. Technol. **2014**, *132*, 33-40.

[15] ASTM D698-12e1.Standard Test Methods for Laboratory Compaction Characteristics of Soil Using Standard Effort (12 400 ft-lbf/ft3 (600 kN-m/m3)). West Conshohocken, Pensilvania, USA. **2012**.

[16] ASTM D2216. Standard test Methods for Laboratory Determination of Water (Moisture) Content of Soil and Rock by Mass. West Conshohocken, Pensilvania, USA. **2010**.

[17] ASTM D854. Standard Test Methods for Specific Gravity of Soil Solids by Water Pycnometer. West Conshohocken, Pensilvania, USA. 2014

[18] ASTM D2487. Classification of Soils for Engineering Purposes (Unified Soil Classification System). West Conshohocken, Pensilvania, USA. **2006**.

[19] Grundl, T.; Michalski, P. Electroosmotically driven water flow in sediments. Water Res. **1996**, *30*, 811-818.

[20] Miller, C.J. Field Investigation of Clay Liner Movement. *H*azard. Waste Hazard. Mater. **1988**, *5*, 231-238.

[21] Montgomery, R.J.; L.J. The Omega Hills Final Cap Test Plot Study: Three Year Data Summary. In *Annual Meeting of the National Solid Waste Management Association*, Washington D.C, 1989.

[22] Daniel, D.E. Soils Used in Cover Systems. In *Design and Construction of RCRA/CERCLA Final Covers*. United States Environmental Protection Agency. **1991,** *145*.

[23] Tang, C.-S.; Shi, B.; Liu, C.; Suo, W.-B.; Gao, L. Experimental characterization of shrinkage and desiccation cracking in thin clay layer. Appl. Clay Sci. **2011**, *52*, 69-77.

[24] Albrecht, B.A.; Benson, C.H. Effect of desiccation on compacted natural clays. J. Geotech. Geoenviron. **2001**, *127*, 67-75.

[25] Boynton, S.S.; Daniel, D.E. Hydraulic Conductivity Tests On Compacted Clay. J. Geotech. Eng-Asce. **1985**, *111*, 465-478.

[26] Casagrande, L. Electro-osmosis in soils. Geotechnique. **1949**, *1*, 159-177.

[27] Mitchell, J.K. *Fundamentals of Soil Behaviour.* 2nd Ed. Wiley: New York, USA. **1993**.

[28] Yeung, A.T.; Mitchell, J.K. Coupled fluid, electrical and chemical flows in soil. Geotechnique, **1993**, *43*, 121-134.

[29] Corte, A.; Higashi, A. Experimental research on desiccation cracks in soil. U.S. Army Snow ice and permafrost research establishment. *Research report 66.* Wilmette, Illinois, USA. **1960**.

[30] Rodriguez, R.; Sanchez, M.; Ledesma, A.; Lloret, A. Experimental and numerical analysis of desiccation of a mining waste. Can. Geotech. J. **2007**, *44*, 644-658.

[31] Yanful, E.K.; Mousavi, S.M.; Yang, M.D. Modeling and measurement of evaporation in moisture-retaining soil covers. Adv. Environ. Res. **2003**, *7*, 783-801.

[32] Fell, R.; Wan, C.F.; Cyganiewicz, J.; Foster, M. Time for development of internal erosion and piping in embankment dams. J. Geotech. Geoenviron. **2003**, *129*, 307-314.

[33] Meyer, P.D.; Rockhold, M.L.; Gee, G.W. Uncertainty Analyses of Infiltration and Subsurface Flow and Transport for SDMP Sites. *Pacific Northwest National Laboratory. U.S. Nuclear Regulatory Commission.*. **1997**.

[34] Barbour, S.L.; Fredlund, D.G. Mechanisms of osmotic flow and volume change in clay soils. Can. Geotech. J. **1989**, *26*, 551-562.

[35] United States Bureau of Reclamation (USBR). Design standards *13*. Embankment dams **1993**.

CAPTIONS

Figure 1. (A) Experimental setup, and (B), mock-up general scheme, and location of instrumentation.

Figure 2. Soil preparation process. (A) Soil compaction procedure through an adapted U.S. Army Corps of Engineers compaction hammer and (B) sampling of soil to corroborate the initial properties.

Figure 3. (A) Water air-water interface meniscus generated between soil particles and tensile stress developed in the upper layer and (B) surface crack initiated. Shown in the figure are: (C), clay particle, (W) pore water and (M) Water-air interface/meniscus. Adapted from Tang et al. [23].

Figure 4. Crack development on the "Sagra soil" mock-up. (A) Surfactant wells and (B), the crack concentration area. Experimental conditions. E_z: 1 V cm^{-1}; Anolyte: Water, Catholyte: Water; Enhancement Fluid: SDS solution (10 kg m^{-3}). Level of soil pollution: 500 mg PHE kg^{-1} dry soil.

Figure 5. Monitorization of Temperature in the "Sagra soil" mock-up. Experimental conditions. E_z: 1 V cm^{-1}; Anolyte: Water, Catholyte: Water; Enhance Fluid: SDS solution (10 kg m^{-3}). Level of soil pollution: 500 mg PHE kg^{-1} dry soil.

Figure 6. Electroosmotic and Gravitational flow evolution in the "Sagra soil" mock-up. Experimental conditions. E_z: 1 V cm^{-1}; Anolyte: Water, Catholyte: Water; Enhance Fluid: SDS solution (10 kg m^{-3}). Level of soil pollution: 500 mg PHE kg^{-1} dry soil.

Figure 7. (A) Moisture restabilization (B) Filling and reparation of the cracks and (C) granular cover arranged on the compacted "Sagra soil" mock-up.

Figure 8. 2-D map (plan view) of the average final dry density distribution in the "Sagra soil" mock-up.

Figure 9. Piping around the surfactant well in the Kaolin mock-up. E_z: 1 V cm^{-1}; Anolyte: Water, Catholyte: Water; Enhance Fluid: SDS solution (10 kg m^{-3}). Level of soil pollution: 500 mg PHE kg^{-1} dry soil.

Figure 10. Cumulative particle size distribution of Kaolin, and "Sagra soil". See table 1 for the soil identification. Distributions were obtained using a laser diffraction particle size analyzer.

Figure 11. (A) Piping generation (highlighted region) around the surfactant addition well in the modified proctor mold test without sand filter and (B) intact soil with the sand filter around the surfactant addition well.

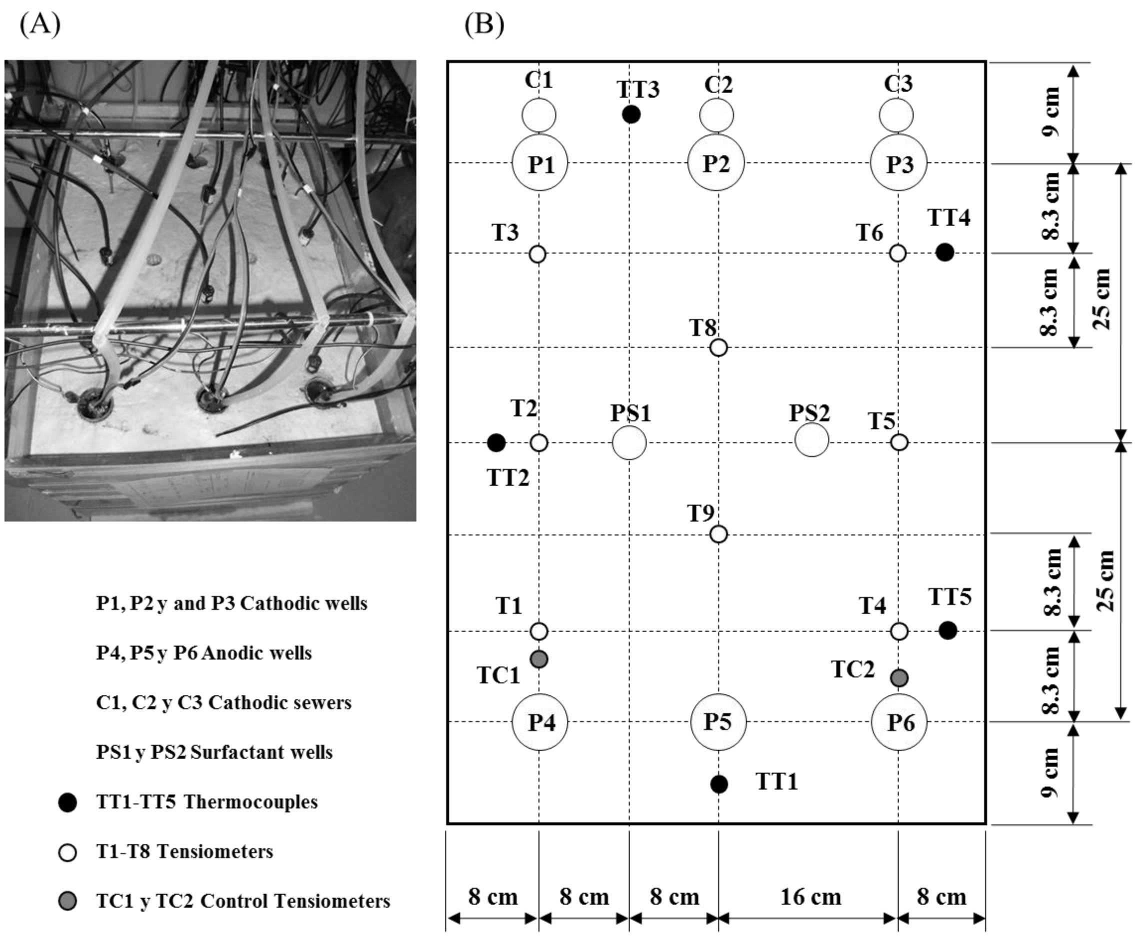
(A)
(B)
C1
TT3
C2
C3
9 cm
P1
P2
P3
8.3 cm
T3
T6
TT4
8.3 cm
25 cm
T8
T2
PS1
PS2
T5
TT2
T9
8.3 cm
25 cm
T1
T4
TT5
TC1
TC2
8.3 cm
P4
P5
P6
9 cm
TT1
8 cm
8 cm
8 cm
16 cm
8 cm
P1, P2 y and P3 Cathodic wells
P4, P5 y P6 Anodic wells
C1, C2 y C3 Cathodic sewers
PS1 y PS2 Surfactant wells
TT1-TT5 Thermocouples
T1-T8 Tensiometers
TC1 y TC2 Control Tensiometers

Fig. 1

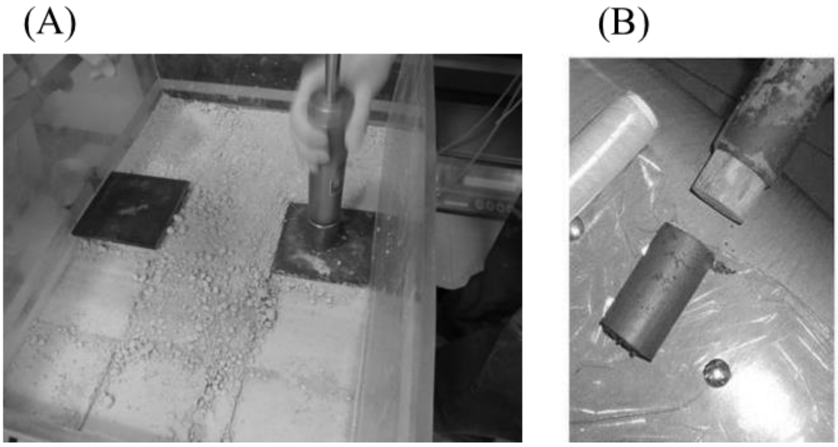

Fig. 2

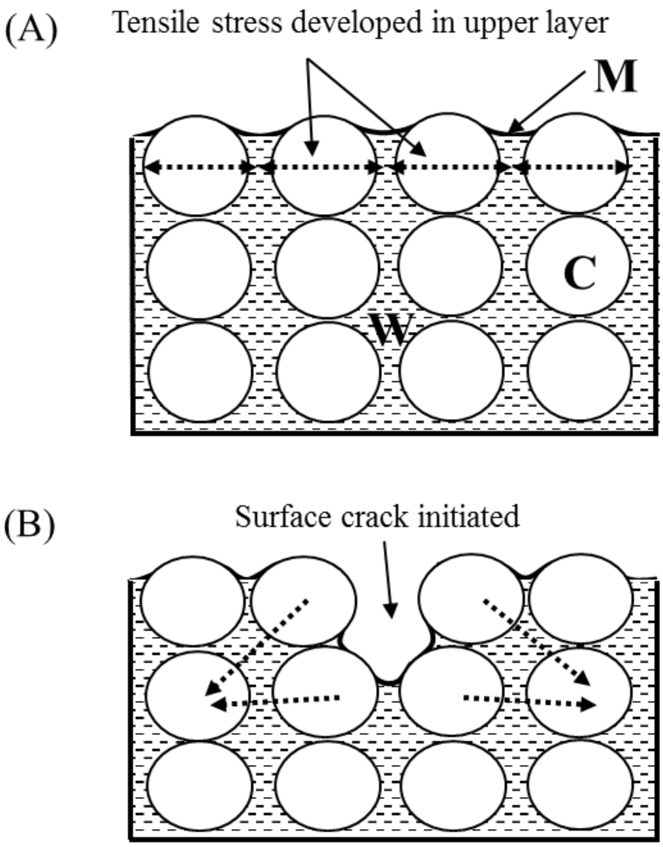
(A)
Tensile stress developed in upper layer
M
C
W
(B)
Surface crack initiated

Fig. 3

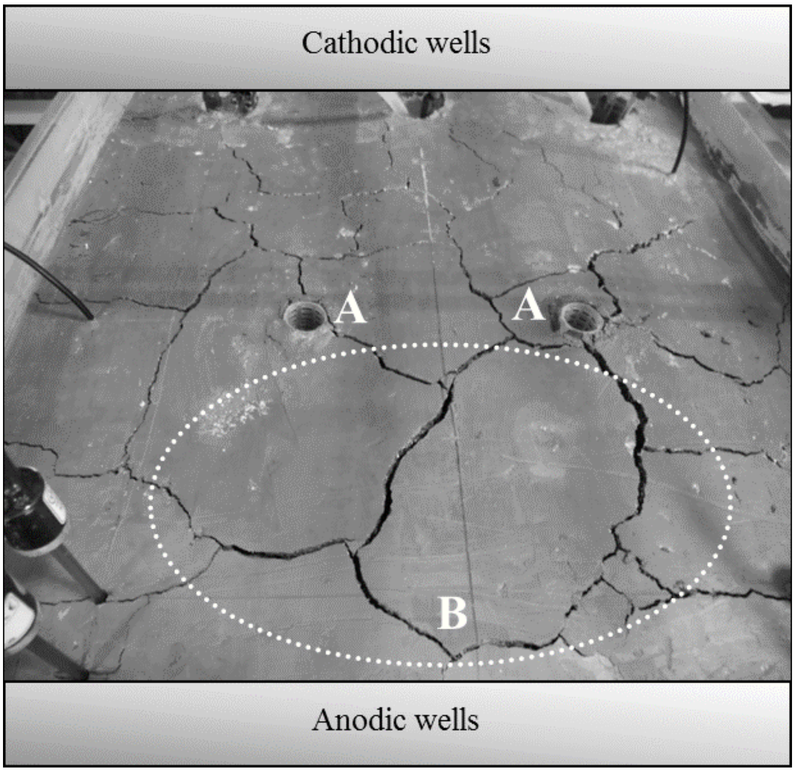

Fig. 4

526 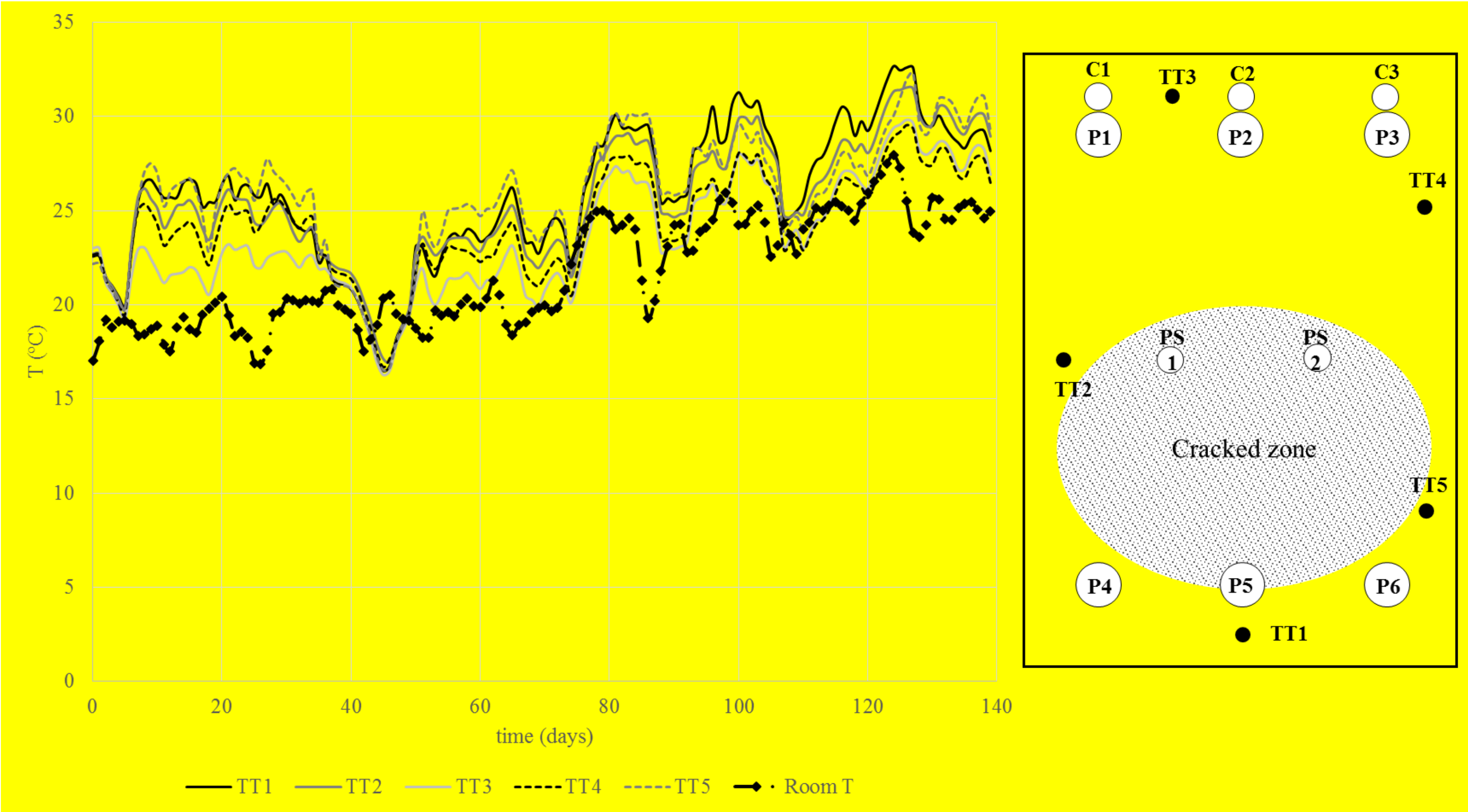

527 Fig. 5

528

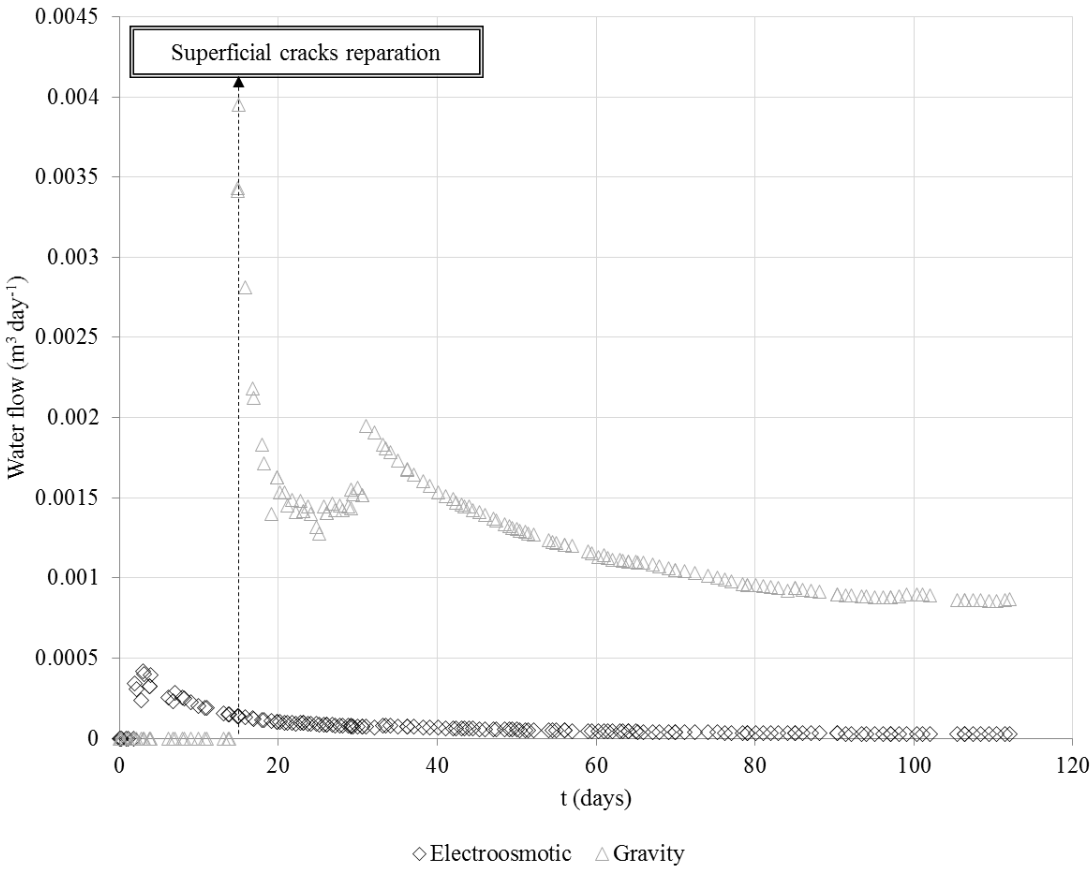

Superficial cracks reparation
Water flow (m3 day-1)
0.0045
0.004
0.0035
0.003
0.0025
0.002
0.0015
0.001
0.0005
0
0
20
40
60
80
100
120
t (days)
Electroosmotic
Gravity

Fig. 6

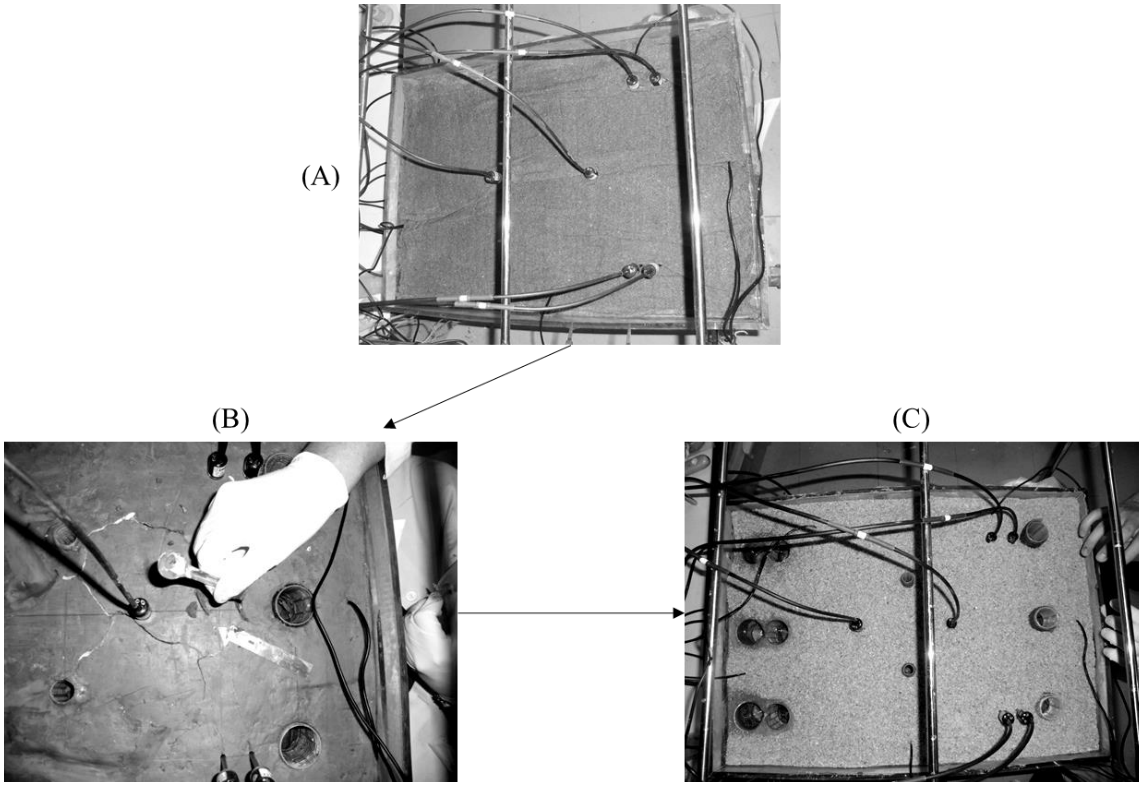

Fig. 7

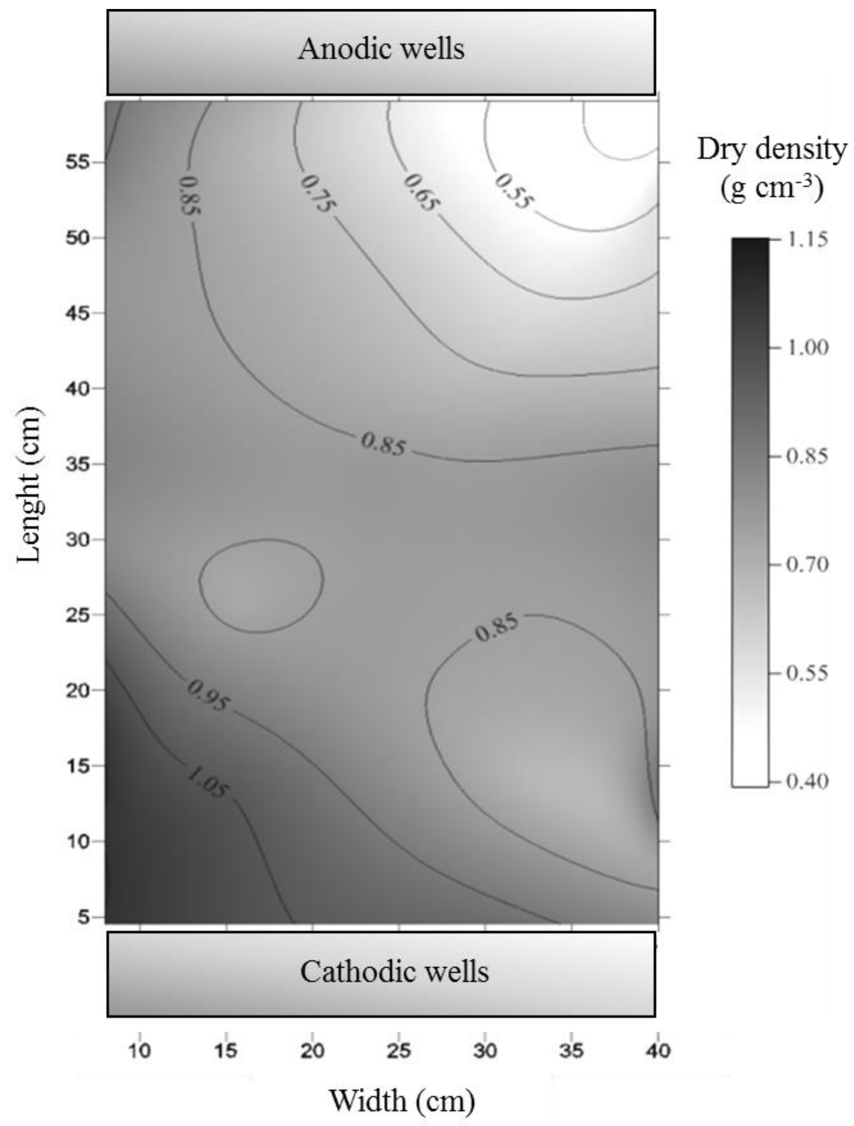
Anodic wells
Dry density
(g cm-3)
1.15
1.00
0.85
0.70
0.55
0.40
0.85
0.75
0.65
0.55
0.85
0.85
0.95
1.05
Lenght (cm)
55
50
45
40
35
30
25
20
15
10
5
Cathodic wells
10
15
20
25
30
35
40
Width (cm)

Fig. 8

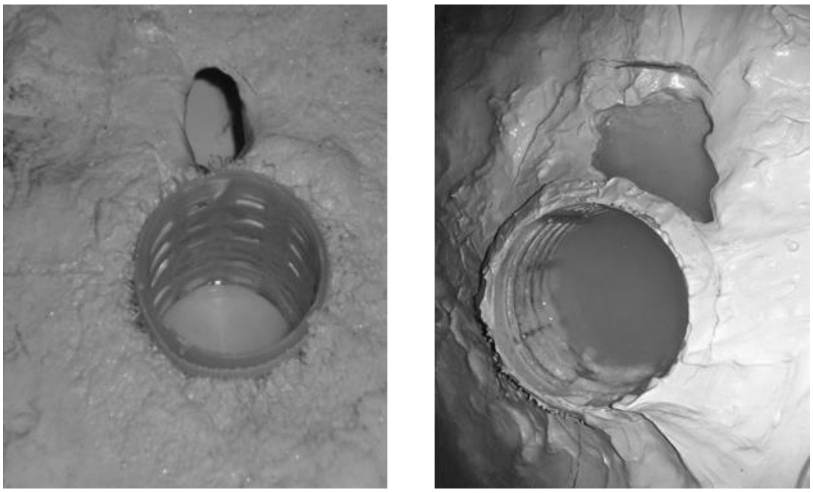

Fig. 9

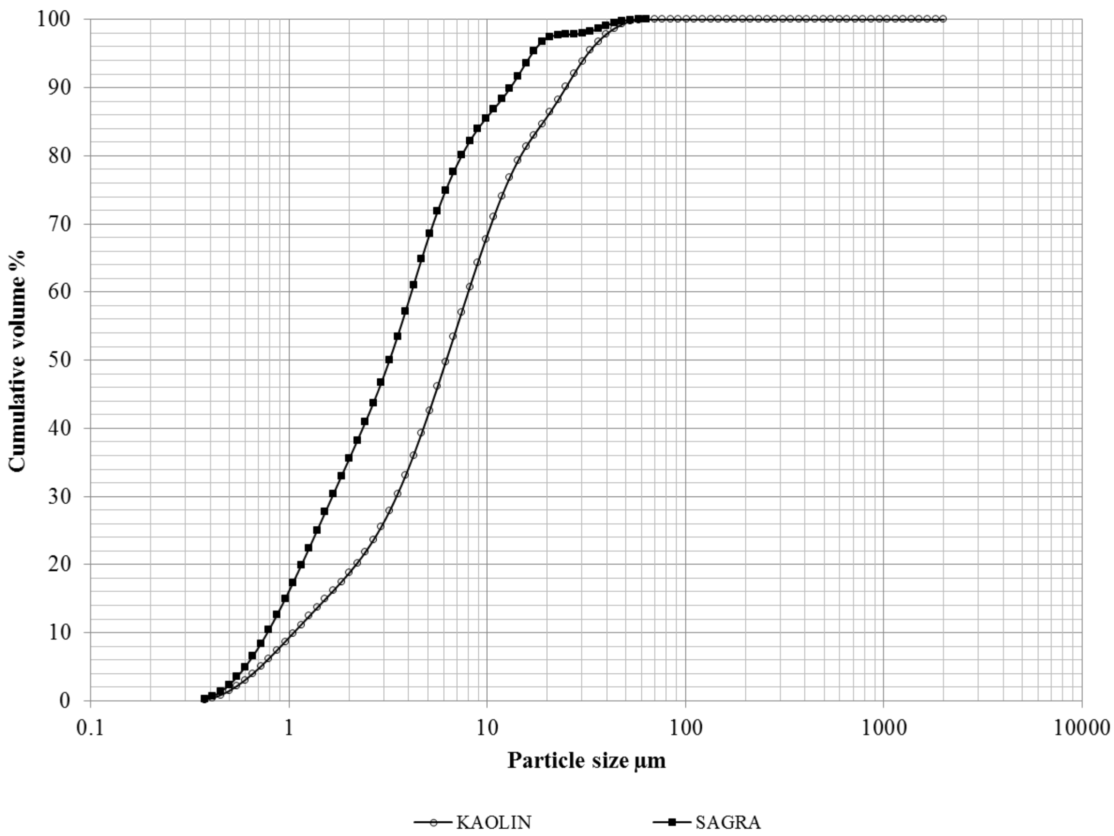
Cumulative volume %
100
90
80
70
60
50
40
30
20
10
0
0.1
1
10
100
1000
10000
Particle size µm
KAOLIN
SAGRA

Fig. 10

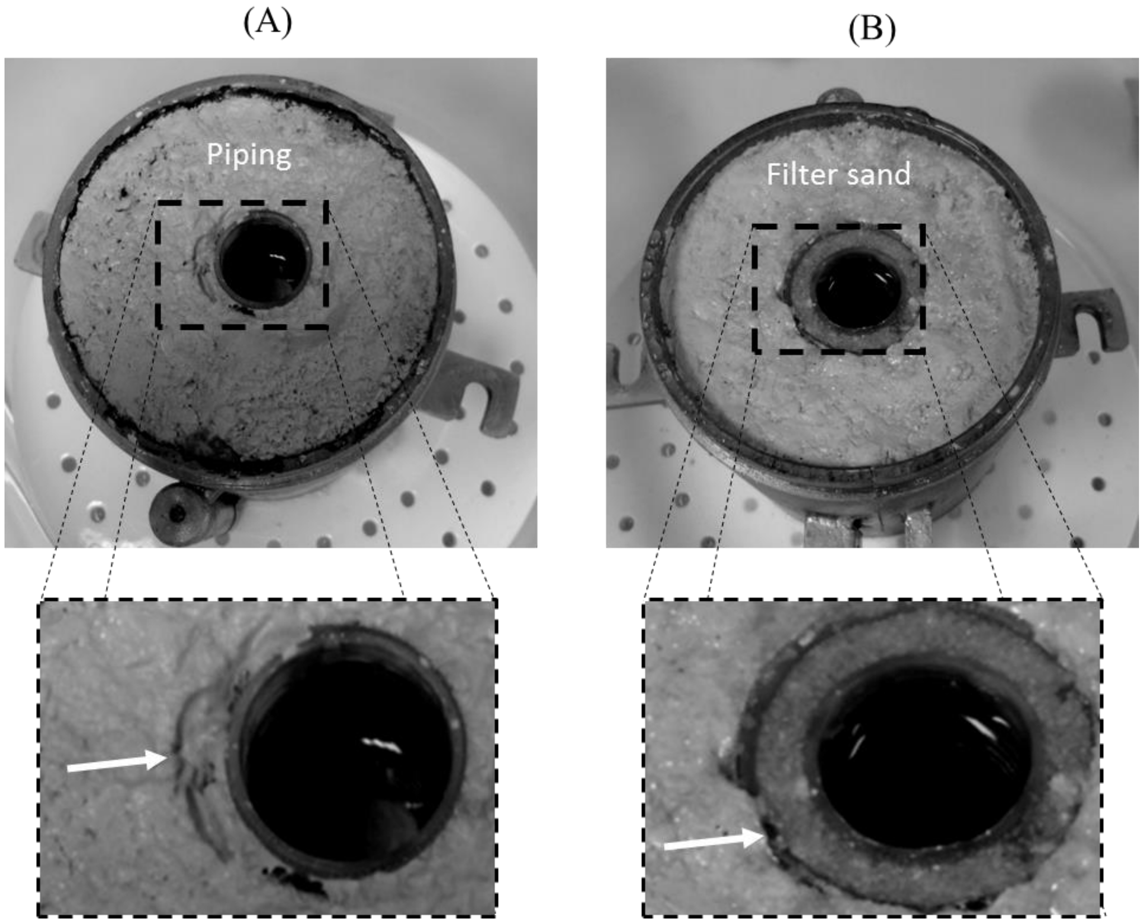

Fig. 11

Table 1. Mineralogical composition of the soils.

	Kaolin[1]	Sagra[2]
Mineral	%	%
Quartz	-	7
Feldspar	-	15
Calcite	-	4
Kaolinite	100	26
Glauconite	-	-
Muscovite	<0.1	-
Montmorillonite	-	-
Smectite	-	28
Illite	<0.1	20

[1]Provided by Productos químicos Manuel Riego S.A.
[2]Provided by Cerámicas Mazarrón S.A.

Table 2. Initial properties of the soil employed in the mock-ups.

Initial soil properties		
Soil	Kaolin	Sagra
***M* (kg)**	122.4	118.3
w_0 (%)	24	29
ρ_s (kg/m^3)	2638	2712
ρ_d (kg/m^3)	1220	1210
***Sr* (%)**	82.9	92.8
e	0.76	0.83
n	0.43	0.45
K_0 (m/s) x 10^{-10}	1.81	2.29
Classification parameters		
Liquid Limit (LL)	41	68
Plastic Limit (PL)	28	28
Plasticity index (PI)	13	40
USCS (ASTM, 2006)	ML/OL	CH

M, mass of soil
K_0, initial hydraulic conductivity

Table 3. Initial and final properties of the Sagra soil.

Parameters	Initial	Final
ρ_d (Kg m^{-3})	1210	820
w (%)	29	34
e	1.19	2.19
n	0.54	0.68
S_r (%)	63.91	40.85

Table 4. Allowable Global-seepage Gradients for concrete Dams on Pervious Foundations (from Meyer et al. [33]).

Soil type	**Allowable Global Gradient**
Very fine sand or silt	0.12
Fine sand	0.14
Medium sand	0.17
Coarse sand	0.20
Fine gravel	0.25
Medium gravel	0.29
Coarse gravel, including cobbles	0.33
Boulders with some cobbles and gravel	0.40
Compact (hard) clay	0.56